Monte Carlo simulations of electromagnetic wave scattering from a random rough surface with three-dimensional penetrable buried object: mine detection application using the steepest-descent fast multipole method

Magda El-Shenawee

Department of Electrical Engineering, University of Arkansas, Fayetteville, Arkansas 72701

Carey Rappaport and Michael Silevitch

Center for Subsurface Sensing and Imaging Systems, Department of Electrical and Computer Engineering, Northeastern University, Room 302 ST, Boston, Massachusetts 02115

Received December 19, 2000; revised manuscript received March 30, 2001; accepted May 16, 2001

We present a statistical study of the electric field scattered from a three-dimensional penetrable object buried under a two-dimensional random rough surface. Monte Carlo simulations using the steepest-descent fast multipole method (SDFMM) are conducted to calculate the average and the standard deviation of the near-zone scattered fields. The SDFMM, originally developed at the University of Illinois at Urbana–Champaign, has been modified to calculate the unknown surface currents both on the rough ground and on the buried object that are due to excitation by a tapered Gaussian beam. The rough ground medium used is an experimentally measured typical dry Bosnian soil with 3.8% moisture, while the buried object represents a plastic land mine modeled as an oblate spheroid with dimensions and burial depth smaller than the free-space wavelength. Both vertical and horizontal polarizations for the incident waves are studied. The numerical results show that the TNT mine signature is almost 5% of the total field scattered from the ground. Moreover, relatively recognizable object signatures are observed even when the object is buried under the tail of the incident beam. Interestingly, even for the small surface roughness parameters considered, the standard deviation of the object signature is almost 30% of the signal itself, indicating significant clutter distortion that is due to the roughness of the ground.

OCIS codes: 290.5880, 290.0290, 280.0280, 280.5600, 350.5500, 350.7420.

1. INTRODUCTION

For subsurface sensing applications such as that indicated in Fig. 1, electromagnetic wave scattering from rough ground is a major source of clutter for the measurements. Analyzing and characterizing this clutter are vital in the development of more efficient radar sensing systems. This random scattering of the electromagnetic fields necessitates the use of Monte Carlo simulations and makes it a key stochastic process in obtaining the statistics of the scattered field and hence in extracting information and drawing meaningful conclusions from the numerical results. There is much published work on electromagnetic scattering from one-dimensional (1-D) or two-dimensional (2-D) random rough surfaces only (without buried objects) using Monte Carlo simulations (e.g., Refs. 1–5). Moreover, there are several publications that model electromagnetic waves from objects buried under 1-D random rough surfaces (e.g., Refs. 6–8) or objects buried under flat half-spaces.[9] However, there are very few published works for an object buried under a 2-D random rough surface; Ref. 10 attempts to model a perfect electrically conducting buried object, and, to the author's knowledge, Ref. 11 is the only attempt to model the case of a penetrable buried object.

The computational expenses, the CPU time, and the computer memory required to calculate the scattering fields from three-dimensional (3-D) penetrable scatterers become excessive for either an electrically large scatterer and/or a scatterer with large dielectric constant. In addition, Monte Carlo simulations require that the calculations be repeated for many rough surface realizations (depending on the ground roughness) until results converge. As is known, solving a 3-D scattering problem is expensive even for one surface realization, so conducting Monte Carlo simulations with hundreds of realizations without using fast algorithms is prohibitive even with supercomputers. Implementing the fast multipole method (FMM)[12–16] makes the solution of a 3-D problem tractable with significant reduction in CPU time and computer memory. The integral-equation-based steepest-descent FMM (SDFMM), a hybridization of the moment method (MOM), the FMM, and the steepest-descent path integra-

0740-3232/2001/123077-08$15.00

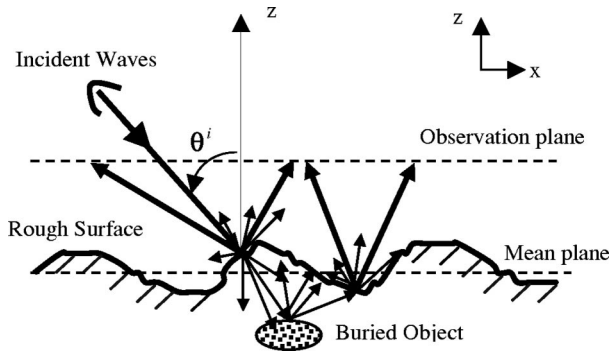

Fig. 1. Cross section of 2-D rough surface ground with 3-D object buried under the interface.

tion rule, is used to calculate the unknown surface currents. The details of the SDFMM are published in Refs. 17–20.

In this work, we are using the same formulations that we developed in Ref. 11, with primary emphasis on conducting efficient and fast Monte Carlo simulations to obtain the statistics of the scattered near fields. In Section 2, the problem formulations are briefly summarized. Numerical results using the SDFMM are presented in Section 3. Conclusions and future work are stated in Section 4.

2. PROBLEM FORMULATION

The SDFMM makes use of the equivalence theorem to calculate the electric and magnetic fields inside and outside a 3-D penetrable object buried under the rough surface interface: details are presented in Ref. 11. The 3-D arbitrary object is modeled by a scatterer R_3 that is immersed in a scatterer R_2, which represents the rough ground. The scatterer R_2 is immersed in the free-space region represented by R_1, as shown in Fig. 2. The three regions, R_1, R_2, and R_3, have permittivity and permeability given by ε_1 and μ_1, ε_2 and μ_2, and ε_3 and μ_3, respectively, representing free space, soil medium, and penetrable buried object. There are two final sets of unknown equivalent electric and magnetic surface currents in the following formulations. They are $\mathbf{J}_1$, $\mathbf{M}_1$, on the exterior of S_1, the interface between R_1 and R_2, and $\mathbf{J}_3$, $\mathbf{M}_3$ on the exterior of S_2, the interface between R_2 and R_3. Upon applying the boundary conditions, continuity of tangential components of the electric and magnetic fields on S_1 and S_2, we obtain new integral equation formulations[11]:

$$\mathbf{E}^{\text{inc}}(\mathbf{r})|_{\text{tang.}} = [(L_1 + L_2)\mathbf{J}_1 - (K_1 + K_2)\mathbf{M}_1 - L_3\mathbf{J}_3 + K_3\mathbf{M}_3]_{\text{tang.}}, \tag{1}$$

$$\mathbf{H}^{\text{inc}}(\mathbf{r})|_{\text{tang.}} = \left[(K_1 + K_2)\mathbf{J}_1 + \left(\frac{L_1}{\eta_1^{\,2}} + \frac{L_2}{\eta_2^{\,2}}\right)\mathbf{M}_1 - K_3\mathbf{J}_3 - \frac{L_3}{\eta_2^{\,2}}\mathbf{M}_3\right]_{\text{tang.}}, \tag{2}$$

$$0 = [-L_2\mathbf{J}_1 + K_2\mathbf{M}_1 + (L_3 + L_4)\mathbf{J}_3 - (K_3 + K_4)\mathbf{M}_3]_{\text{tang.}}, \tag{3}$$

$$0 = \left[-K_2\mathbf{J}_1 - \frac{L_2\mathbf{M}_1}{\eta_2^{\,2}} + (K_3 + K_4)\mathbf{J}_3 + \left(\frac{L_3}{\eta_2^{\,2}} + \frac{L_4}{\eta_3^{\,2}}\right)\mathbf{M}_3\right]_{\text{tang.}}, \tag{4}$$

where the integrodifferential operators L_i and K_i, $i = 1, 2, 3, 4$, are given in detail in Ref. 11. In Eqs. (1)–(4), the unknown surface electric and magnetic currents are $\mathbf{J}_1$, $\mathbf{M}_1$, $\mathbf{J}_3$, and $\mathbf{M}_3$, while the tangential components of the incident electric and magnetic fields on the rough surface are given by $\mathbf{E}^{\text{inc}}(\mathbf{r})|_{\text{tang.}}$ and $\mathbf{H}^{\text{inc}}(\mathbf{r})|_{\text{tang.}}$, respectively. The intrinsic impedance in each region is $\xi_1 = \sqrt{\mu_i/\varepsilon_i}$, $i = 1, 2, 3$, where the dielectric permittivity and permeability in each region are ε_i and μ_i, respectively. Equations (1)–(4) are considered the extension of the Poggio–Miller–Chang–Harrington–Wu formulation, which has been shown to yield a unique solution at internal resonances associated with the corresponding conducting scatterer.[21–23] The equivalent electric and magnetic currents are approximated by using the Rao–Wilton–Glisson vector basis functions $\mathbf{j}(\mathbf{r})$ (Refs. 21 and 24):

$$\mathbf{J}_1(\mathbf{r}) = \sum_{n=i}^{N} I_{1n}\mathbf{j}_{1n}(\mathbf{r}),$$

$$\mathbf{M}_1(\mathbf{r}) = \xi_1 \sum_{n=1}^{N} I_{2n}\mathbf{j}_{1n}(\mathbf{r}), \qquad \mathbf{r} \in S_1, \tag{5a}$$

$$\mathbf{J}_3(\mathbf{r}) = \sum_{m=1}^{P} I_{3m}\mathbf{j}_{2m}(\mathbf{r}),$$

$$\mathbf{M}_3(\mathbf{r}) = \xi_1 \sum_{m=1}^{P} I_{4m}\mathbf{j}_{2m}(\mathbf{r}), \qquad \mathbf{r} \in S_2, \tag{5b}$$

where surfaces S_1 and S_2 are discretized into triangular patches with total number of edges (number of unknown coefficients) equal to N on S_1 and equal to P on S_2. As shown in Eqs. (5), both the electric and magnetic surface currents have the same number of unknown coefficients (edges) on each surface. If we apply Galerkin's method and substitute the above current approximations into

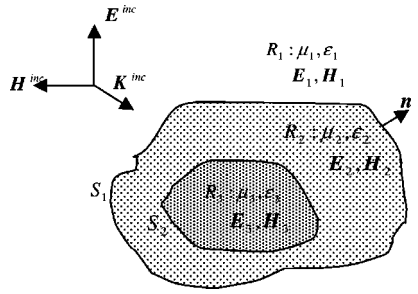

Fig. 2. Penetrable 3-D scatterer R_3 immersed in scatterer R_2 immersed in region R_1.

Eqs. (1)–(4), the original integral equations are transformed into a set of linear system of equations given by

$$\mathbf{ZI} = \mathbf{V}. \tag{6}$$

Note that the matrix $\mathbf{Z}$ has order $2(N + P) \times 2(N + P)$, and that the vector $\mathbf{V}$ is a matrix of order $2(N + P) \times 1$, composed of a submatrix of the tested tangential incident electric field $\mathbf{E}^{\text{inc}}$ of order $N \times 1$, a submatrix of the tested normalized magnetic field $\eta_1 \mathbf{H}^{\text{inc}}$ of order $N \times 1$, and a null submatrix of order $2P \times 1$. Finally, the SDFMM is implemented in Eq. (6), reducing the computational complexity for the CPU time and computer memory requirements from $O(K^2)$ for the MOM to only $O(K)$ per iteration of iterative solver for the SDFMM,[17–19] where $K = 2(P + N)$ is the total number of the electric and magnetic surface current unknowns.

3. NUMERICAL RESULTS

The SDFMM code has been validated with the sparse canonical conjugate gradient method,[10] where the scatterer is a perfect electrically conducting sphere buried under a random rough surface, and good agreement is presented in Ref. 11. More validations of the SDFMM code (not presented here) have been conducted, showing excellent agreement between the SDFMM code and both the Mie and MOM solutions for the case of just a penetrable sphere immersed in air (no rough surface) and excited by an incident plane wave.[21]

In all the results presented in this section, the incident wave is assumed to be a Gaussian beam[25] located in the plane of incidence, as shown in Fig. 1. The half-beam width of the Gaussian beam is assumed to be $L/5$, where the simulated rough ground has dimensions equal to $L \times L$, with $L = 8\lambda_0$ in this work. This leads to plane-wave illumination of a spot size of diameter $3.2\lambda_0$ on the ground with tapered illumination toward the edges of the finite modeled ground. The rough surface is characterized with Gaussian statistics for the random heights and for the autocorrelation function. In this work, we are interested in the antipersonnel mine detection application, which justifies the assumption of small roughness parameters of the ground given by the root-mean-square height $\sigma = 0.04\lambda_0$ and the correlation length $l_c = 0.5\lambda_0$. The dielectric constant of a typical Bosnian soil with 3.8% moisture is $\varepsilon_r = 2.5 - i0.18$ at 1 GHz,[26] while the dielectric constant of the buried object (TNT material) is $\varepsilon_r = 2.9 - i0.072$. The buried object is modeled as an oblate spheroid with top view as a circle of radius $a = 0.3\lambda_0$ and both front and side views as ellipses of dimensions $a = 0.3\lambda_0$ and $b = 0.15\lambda_0$. The burial depth of the object is $d = 0.3\lambda_0$ and is measured from its center to the mean plane of the rough surface. In this work, the incident Gaussian beam is always pointing at the center of the rough ground, with plane-wave illumination spot diameter equal to $3.2\lambda_0$ compared with the $0.6\lambda_0$ diameter of the buried spheroid. Moreover, all the results here represent scattered near electric fields, and all subtraction processes are conducted with complex vectors.

In all the results in this section, the discretization length of the surface current on the rough ground is assumed to be $0.08\lambda_0$, producing a total number of surface current unknowns of $2N = 59{,}600$.[11] The number of nodes and patches on the buried penetrable oblate spheroid is 122 and 240, respectively, producing a total number of surface current unknowns of $2P = 720$.[11] The dimensions of the SDFMM finest block are assumed to be $0.32\lambda_0 \times 0.32\lambda_0$, with two blocks separating the near-field (MOM) interactions from the far-field (SDFMM) interactions on the scatterer.[17–19]

As mentioned above, we are primarily interested in scattered electric fields in the near zone, which can be calculated by using the solved electric and magnetic surface currents[27] and are obtained at point receivers located $0.5\lambda_0$ above the nominal rough surface with resolution $0.1\lambda_0$, as shown in Fig. 1. The magnitude of the average

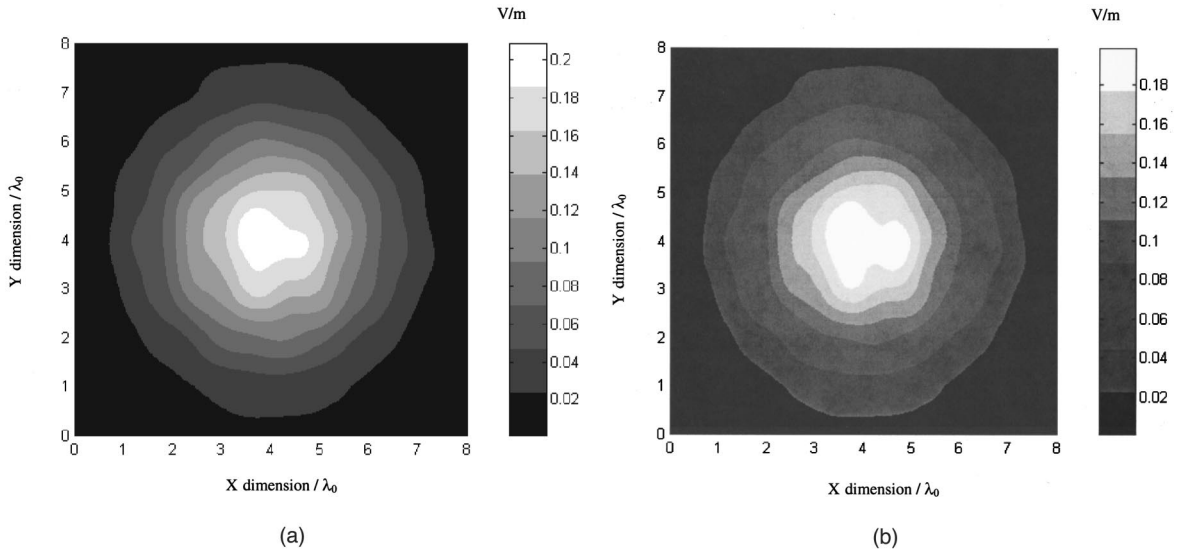

Fig. 3. (a) Average of near electric field scattered at $z = 0.5\lambda_0$ above rough ground of rms height $\sigma = 0.04\lambda_0$ and correlation length $l_c = 0.5\lambda_0$ with incidence angle $\theta^i = 0°$ for horizontal polarization. (b) Average of near electric field scattered at $z = 0.5\lambda_0$ above rough ground of rms height $\sigma = 0.04\lambda_0$ and correlation length $l_c = 0.5\lambda_0$ with incidence angle $\theta^i = 0°$ for horizontal polarization. The oblate spheroid object has dimensions $a = 0.3\lambda_0$ and $b = 0.15\lambda_0$ and is buried at depth $d = 0.3\lambda_0$ under the mean plane of the surface.

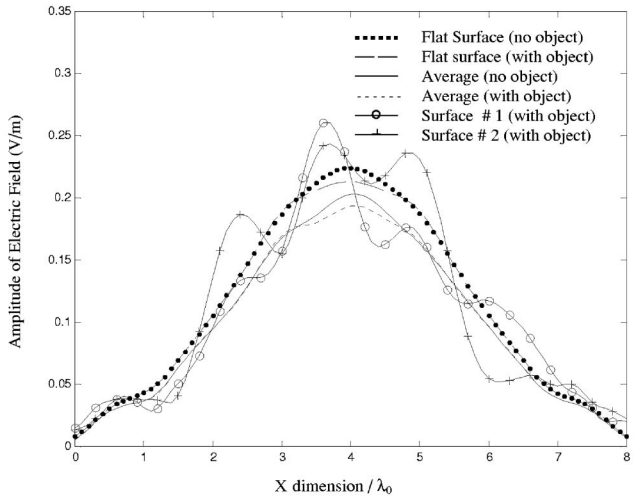

(a)

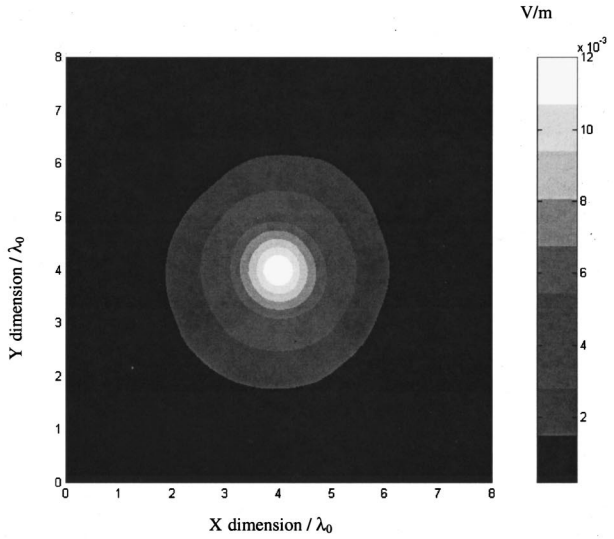

(b)

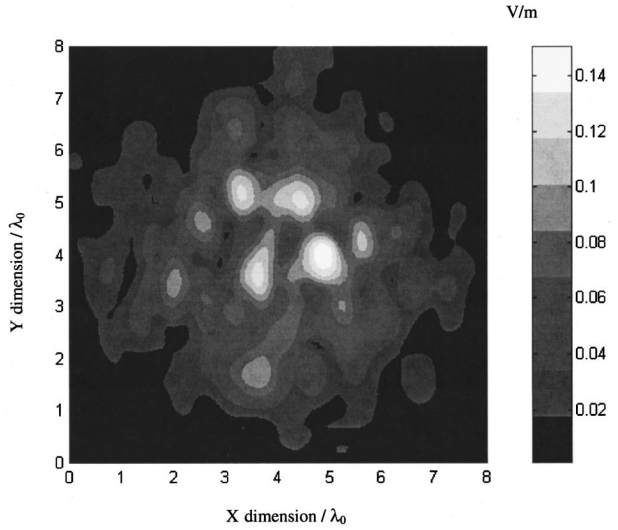

(c)

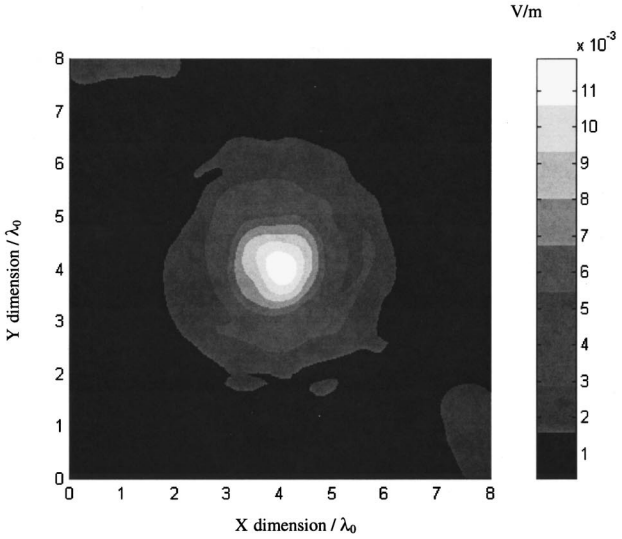

(d)

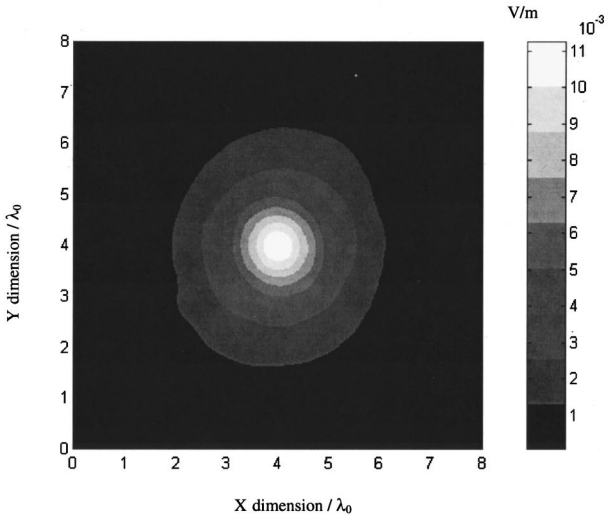

(e)

Fig. 4. Near electric field scattered at $z = 0.5\lambda_0$ (a) from two individual rough surface realizations with buried spheroid selected from Fig. 3(b) (surfaces 1 and 2), the average of 65 electric fields scattered from a rough surface with and without the buried spheroid [Figs. 3(b) and 3(a), respectively], and the scattered electric field from flat ground with and without the buried spheroid, all plotted at $Y = 4.0\lambda_0$; (b) that is due to just the buried object under a flat ground obtained by subtraction; (c) that is due to just the buried object obtained by subtracting the average electric field of Fig. 3(a) from the field scattered from only one surface (with buried spheroid) selected from the 65 realizations used to obtain Fig. 3(b); (d) that is due to just the buried object obtained by subtracting fields scattered from only one surface selected from the 65 realizations used to obtain Fig. 3(a) (surface only) from fields scattered from the same surface (with buried spheroid) selected from the 65 realizations used to obtain Fig. 3(b); (e) average scattered near electric field that is due to just the buried object obtained by subtracting fields scattered from the 65 realizations used to obtain Fig. 3(a) from fields scattered from the same 65 realizations and used to obtain Fig. 3(b) and then take the statistical average. For (a)–(e) the incidence angle is $\theta^i = 0°$ for horizontal polarization, where the spheroid is buried at $x = y = 4.0\lambda_0$, $z = -0.3\lambda_0$.

scattered electric field and the standard deviation (STD) are calculated as

$$\text{Average} = \frac{1}{M}\sum_{i=1}^{M}\mathbf{E}_i, \tag{7a}$$

$$\text{STD} = \left(\frac{1}{M}\sum_{i=1}^{M}|\mathbf{E}_i|^2 - |\frac{1}{M}\sum_{i=1}^{M}\mathbf{E}_i|^2\right)^{1/2}, \tag{7b}$$

where $\mathbf{E}_i$ represents the complex vector electric field scattered from the ith rough surface realization, $i=1, 2, ..., M$, where the size of the Monte Carlo set (M) is assumed to be 65 in all the results in this section.

In Figs. 3–7, two incidence elevation angles with one azimuth angle $\phi^i = 0$ will be considered; $\theta^i = 0$ for the horizontally polarized incident waves where the electric field is in the y direction (Figs. 3–6), and $\theta^i = 10°$ for both polarizations (Fig. 7).

In Figs. 3(a) and 3(b), the magnitude of the average scattered near electric fields at $z = 0.5\lambda_0$, with the use of Monte Carlo simulations, from the rough surface alone and from the rough surface with the buried spheroid, located at $x = y = 4.0\lambda_0$, are shown respectively. Note the slight difference between results in Figs. 3(a) and 3(b), which is due to the small size of the buried object compared with the free-space wavelength. Our objective is to analyze and extract information about the buried object that caused this slight difference. In Fig. 4(a), the scattered near electric fields from the buried spheroid under two individual rough surface realizations selected from the 65 used in Fig. 3(b), the average of the 65 surface realizations of rough surface with buried object [Fig. 3(b)], the average of the 65 surface realizations of rough surface alone [Fig. 3(a)], and the scattered electric field from flat ground with and without buried object are plotted at $Y = 4.0\lambda_0$. The results of Fig. 4(a) show the oscillations in the scattered electric fields from these individual rough surface realizations compared with the smooth curve obtained upon averaging the fields using Monte Carlo simulations. Note that the average fields shown in Fig. 4(a) (solid and dotted curves) are not perfectly symmetrical around the point $X = 4.0\lambda_0$ compared with the symmetrical results of the flat ground. This can be attributed to the relatively small size of the Monte Carlo sample (65 realizations) and to the edge effect of the finite modeled rough ground. This qualitative comparison shown in Fig. 4(a) indicates the significant effect of the rough ground on the scattered signals, even with the small roughness parameters chosen in this application. To obtain the scattered fields that are due just to the buried object, we conducted four types of subtraction with complex vectors, and the results are shown in Figs. 4(b)–4(e). First, we subtract the electric field scattered from flat ground alone from those scattered from flat ground with buried spheroid, and the results are shown in Fig. 4(b). Second, we subtract the average scattered field from rough surface alone [solid curve in Fig. 4(a)] from the fields scattered from one rough surface realization with the buried object [surface 1 in Fig. 4(a)]. The outcome is plotted in Fig. 4(c), which shows very noisy results compared with those in Fig. 4(b). Then, the near electric fields scattered form only one surface realization are subtracted from those scattered from the same surface realization with buried spheroid, and the results are plotted in Fig. 4(d). Significant enhancement in results is shown in Fig. 4(d) compared with Fig. 4(c), giving more information about the object signature. Finally, upon repeating the subtraction process of Fig. 4(d) for each of the 65 rough surface realizations and then taking the statistical average of the outcome, we obtain the results shown in Fig. 4(e). Thus conducting Monte Carlo simulations of the 65 object signals obtained by subtraction gives an ideal image, as clearly shown in Fig. 4(e) compared with Figs. 4(b)–4(d). In practice, signals scattered from a target buried under only one rough ground are measured. However, the statistics shown in Fig. 4(e) are used to conclude that the TNT spheroid has a signature almost equal to 5% of the total scattered fields. In reality, neither the profile of the rough ground nor its soil dielectric constant is precisely known. However, if these parameters can be estimated, then our fast model can be used to compute the scattered fields from the rough ground alone. As a result, it can be used to remove the clutter from the measurement data by subtraction, as shown above, aiming to obtain results similar to those in Fig. 4(d). Signal-processing techniques could be applied to this output rather than directly to the more noisy measurement data.

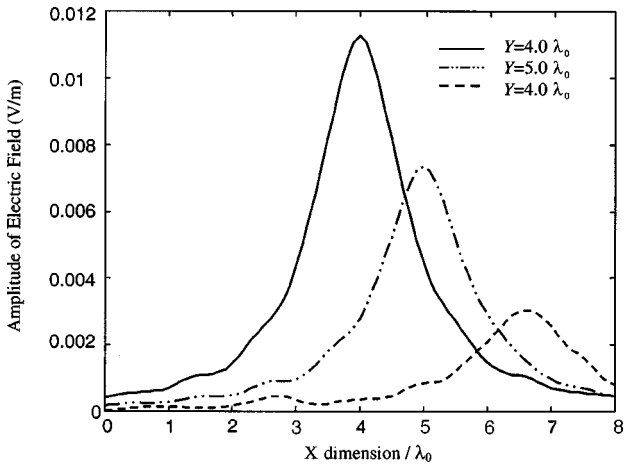

Fig. 5. Comparison between signatures of three objects located at $x = y = 4.0\lambda_0$, $x = y = 5.0\lambda_0$, and $x = 6.5\lambda_0$, $y = 4.0\lambda_0$.

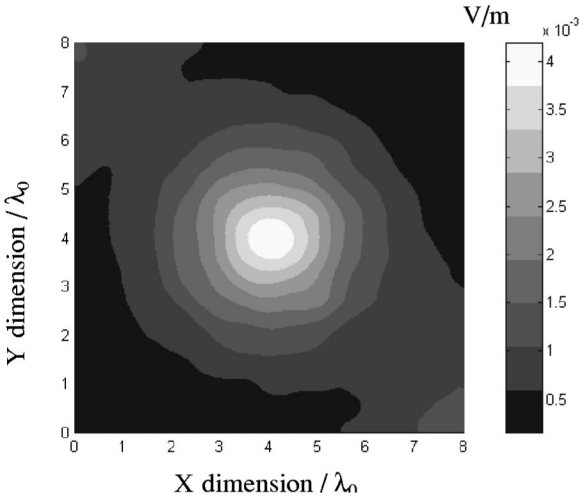

Fig. 6. STD of scattered near electric fields that are due to just the buried spheroid for the same data as those in Fig. 4(e).

If we keep the incident Gaussian beam pointing at the center of the ground and change the location of the buried spheroid from the center of the ground at $x = y = 4.0\lambda_0$ to $x = y = 5.0\lambda_0$ and to $x = 6.5\lambda_0$, $y = 4.0\lambda_0$, results similar to those in Fig. 4(e) are obtained at these locations. A qualitative comparison between the scattered electric fields from the buried spheroid versus the object location is shown in Fig. 5. As expected, these results show the degradation of object signature with respect to its closeness to the center of the incident Gaussian beam. Although the maximum excitation is not over the target, computing the difference fields clearly shows the target position. The STD of the 65 scattered electric fields that are due just to the spheroid is calculated by using Eq. (7b) and plotted in Fig. 6 which shows that it is equal to almost 30% of the object signature shown in Fig. 4(e). In Figs. 7(a) and 7(b), the elevation angle of the incident Gaussian beam is varied to be $\theta^i = 10°$, and the average scattered fields with the use of Monte Carlo simulations are plotted for the vertical polarization from surface only and from surface with buried spheroid, respectively. Also, slight distortion is observed in the object signature at this oblique incidence angle for both polarizations, as shown in Figs. 7(c) and 7(d).

The CPU times required for the SDFMM to calculate the surface current unknowns for each rough surface realization are 38 min to fill in the impedance matrix, 72 min for the transpose-free quasi-minimal residual iterative solver,[28] and 3 min to calculate the near field scattered above the ground with $0.1\lambda_0$ resolution. The com-

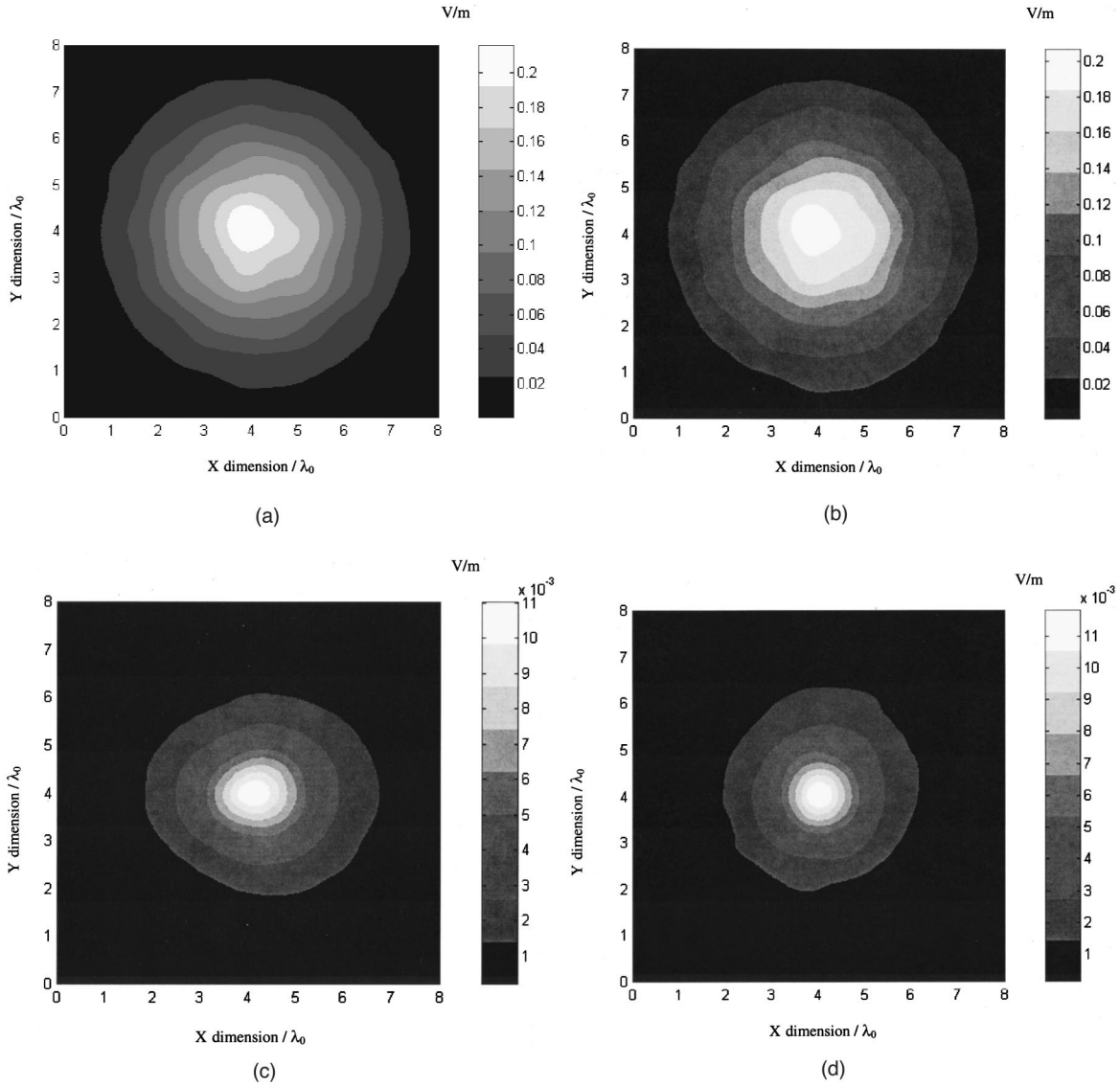

Fig. 7. (a) Average of near electric field scattered at $z = 0.5\lambda_0$ above rough ground of rms height $\sigma = 0.04\lambda_0$ and correlation length $l_c = 0.5\lambda_0$ with incidence angle $\theta^i = 10°$ for vertical polarization. (b) Average of near electric field scattered at $z = 0.5\lambda_0$ above rough ground of rms height $\sigma = 0.04\lambda_0$ and correlation length $l_c = 0.5\lambda_0$ with incidence angle $\theta^i = 10°$ for vertical polarization. The object has dimensions $a = 0.3\lambda_0$ and $b = 0.15\lambda_0$ and is buried at depth $d = 0.3\lambda_0$ under the mean plane of the surface. (c) Average scattered near electric field that is due to just the buried object obtained by subtracting fields scattered from the 65 realizations used to obtain Fig. 7(a) from fields scattered from the same 65 realizations and used to obtain Fig. 7(b) and then by taking the statistical average. The incidence angle is $\theta^i = 10°$ for vertical polarization. (d) Average scattered near electric field that is due to just the buried object for data similar to those shown in Fig. 7(c) but for horizontal polarization.

puter memory required to run the SDFMM is 950 Mbytes. These computations were conducted by using one processor on Compaq GS140 EV6 machine.

As is known, the size of the Monte Carlo sample (number of rough surface realizations) increases dramatically with the increase of ground roughness parameters. For flat ground, only one surface is needed, while for very rough ground, hundreds of realizations are needed for efficient conduction of Monte Carlo simulations. The adequate sample size can be obtained by gradually increasing the number of realizations used in the calculations until no change is observed in numerical results. The CPU time dramatically increases with the increase of Monte Carlo sample size. This barrier can be eliminated by the possible parallel implementation of the SDFMM code similar to the sparse canonical conjugate gradient method.[29]

4. CONCLUSIONS

We demonstrated the implementation of the SDFMM to calculate the unknown surface currents on a random rough surface with buried 3-D penetrable object. The significant speed of this algorithm allowed an efficient conduction of the Monte Carlo simulations. The average and the STD of the near fields scattered from the ground with the buried object are calculated. Our results showed that the presence of the rough interface distorts the scattered fields from the buried object, even for the small roughness parameters considered here. Interestingly, we also showed that the STD statistic of the object signals is large relative to the signal itself. Recognizable object signature is observed even when the object is not buried under the center of the ground where the incident Gaussian beam is pointing. Having determined some of the statistics of both clutter and target signals, one can apply statistical signal processing for target detection, which is the subject of future work.

ACKNOWLEDGMENTS

The authors thank W. Chew, E. Michielssen, and V. Jandhyala at UIUC for allowing them the use and the modification of the SDFMM computer code for the current application. This research was sponsored by U.S. Army Research Office Demining Multi-University Research Initiative grant DAA 0-55-09-0013 and in part by the Engineering Research Centers Program of the National Science Foundation under award EEC-9986821. This work benefited from the allocation of time at the Northeastern University Advanced Scientific Computation Center.

Address correspondence to M. El-Shenawee at the location on the title page or by phone, 501-575-6582; fax, 501-575-7967; or e-mail, magda@uark.edu.

REFERENCES

1. L. Tsang, C. H. Chan, K. Pak, H. Sangani, A. Ishimaru, and P. Phu, "Monte Carlo simulations of large-scale composite random rough-surface scattering based on the banded-matrix iterative approach," J. Opt. Soc. Am. A **11**, 691–696 (1994).
2. R. L. Wagner, J. Song, and W. C. Chew, "Monte Carlo simulation of electromagnetic scattering from two-dimensional random rough surfaces," IEEE Trans. Antennas Propag. **45**, 235–245 (1997).
3. C. H. Chan, L. Tsang, and Q. Li, "Monte Carlo simulations of large-scale one dimensional random rough-surface scattering at near grazing incidence: penetrable case," IEEE Trans. Antennas Propag. **46**, 142–149 (1998).
4. F. D. Hastings, J. B. Schneider, and S. L. Broschat, "A Monte Carlo FDTD technique for rough surface scattering," IEEE Trans. Antennas Propag. **43**, 1183–1191 (1995).
5. J. T. Johnson, L. Tsang, R. T. Shin, K. Pak, C. H. Chan, A. Ishimaru, and Y. Kuga, "Backscattering enhancement of electromagnetic waves from two-dimensional perfectly conducting random rough surfaces: comparison of Monte Carlo simulations with experimental data," IEEE Trans. Antennas Propag. **44**, 748–756 (1996).
6. K. O'Neill, R. F. Lussky, Jr., and K. D. Paulsen, "Scattering from a metallic object embedded near the randomly rough surface of a lossy dielectric," IEEE Trans. Geosci. Remote Sens. **34**, 367–376 (1996).
7. G. Zhang, L. Tsang, and Y. Kuga, "Studies of the angular correlation function of scattering by random rough surfaces with and without a buried object," IEEE Trans. Geosci. Remote Sens. **35**, 444–453 (1997).
8. A. Madrazo and M. Nieto-Vesperinas, "Scattering of light and other electromagnetic waves from a body buried beneath a highly rough random surface," J. Opt. Soc. Am. A **14**, 1859–1866 (1997).
9. N. Geng, A. Sullivan, and L. Carin, "Multilevel fast-multipole algorithm for scattering from conducting targets above or embedded in a lossy half space," IEEE Trans. Geosci. Remote Sens. **38**, 1561–1573 (2000).
10. G. Zhang, L. Tsang, and K. Pak, "Angular correlation function and scattering coefficient of electromagnetic waves scattered by a buried object under a two-dimensional rough surface," J. Opt. Soc. Am. A **15**, 2995–3002 (1998).
11. M. El-Shenawee, C. Rappaport, E. Miller, and M. Silevitch, "3-D subsurface analysis of electromagnetic scattering from penetrable/PEC objects buried under rough surfaces: use of the steepest descent fast multipole method (SDFMM)," IEEE Trans. Geosci. Remote Sens. **39**, 1174–1182 (2001).
12. V. Rokhlin, "Rapid solution of integral equations of scattering theory in two dimensions," J. Comput. Phys. **36**, 414–439 (1990).
13. R. Coifman, V. Rokhlin, and S. Wandzura, "The fast multipole method for the wave equation: a pedestrian description," IEEE Antennas Propag. Mag. **35** (No. 3), 7–12 (1993).
14. C. C. Lu and W. C. Chew, "Fast algorithm for solving hybrid integral equations," IEE Proc. Pt. H **140**, 455–460 (1993).
15. C. C. Lu and W. C. Chew, "A multilevel fast-algorithm for solving a boundary integral equation of wave scattering," Microwave Opt. Technol. Lett. **7**, 466–470 (1994).
16. J. M. Song and W. C. Chew, "Multilevel fast-multipole algorithm for solving combined field integral equations of electromagnetic scattering," Microwave Opt. Technol. Lett. **10**, 14–19 (1995).
17. V. Jandhyala, "Fast multilevel algorithms for the efficient electromagnetic analysis of quasi-planar structures," Ph.D. thesis (Department of Electrical and Computer Engineering, University of Illinois at Urbana-Champaign, Urbana-Champaign, Ill., 1998).
18. V. Jandhyala, E. Michielssen, B. Shanker, and W. C. Chew, "A combined steepest descent–fast multipole algorithm for the fast analysis of three-dimensional scattering by rough surfaces," IEEE Trans. Geosci. Remote Sens. **36**, 738–748 (1998).
19. V. Jandhyala, B. Shanker, E. Michielssen, and W. C. Chew, "A fast algorithm for the analysis of scattering by dielectric rough surfaces," J. Opt. Soc. Am. A **15**, 1877–1885 (1998).
20. M. El-Shenawee, V. Jandhyala, E. Michielssen, and W. C. Chew, "The steepest descent fast multipole method (SDFMM) for solving combined field integral equation pertinent to rough surface scattering," in *Proceedings of the IEEE APS/URSI '99 Conference* (Institute of Electrical and Electronics Engineers, New York, 1999), pp. 534–537.

21. L. Medgyesti-Mitschang, J. Putnam, and M. Gedera, "Generalized method of moments for three-dimensional penetrable scatterers," J. Opt. Soc. Am. A **11**, 1383–1398 (1994).
22. J. R. Mautz and R. F. Harrington, "H-field, E-field, and combined field solutions for conducting bodies of revolutions," Arch. Elektr. Uebertrag. **32**, 157–164 (1978).
23. P. L. Huddleston, L. N. Medgyesi-Mitschang, and J. M. Putnam, "Combined field integral equation formulation for scattering from dielectrically coated conducting bodies," IEEE Trans. Antennas Propag. **AP-34**, 510–520 (1986).
24. S. M. Rao, D. R. Wilton, and A. W. Glisson, "Electromagnetic scattering by surfaces of arbitrary shape," IEEE Trans. Antennas Propag. **AP-30**, 409–418 (1982).
25. P. Tran and A. A. Maradudin, "Scattering of a scalar beam from a two-dimensional randomly rough hard wall: enhanced backscatter," Phys. Rev. B **45**, 3936–3939 (1992).
26. J. Curtis, "Dielectric properties of soils; various sites in Bosnia," Station Data Rep. (U.S. Army Corps of Engineers, Waterways Experiment, Washington, D.C., 1996).
27. C. A. Balanis, *Advanced Engineering Electromagnetics* (Wiley, New York, 1989), Chap. 6, pp. 254–309.
28. R. W. Freund, "A transpose-free quasi-minimal residual algorithm for non-Hermitian linear systems," SIAM J. Sci. Comput. **14**, 470–482 (1993).
29. S. Li, C. H. Chan, L. Tsang, Q. Li, and L. Zhou, "Parallel implementation of the parse matrix/canonical grid method for the analysis of two-dimensional random rough surfaces (three-dimensional scattering problem) on a Beowulf system," IEEE Trans. Geosci. Remote Sens. **38**, 1600–1608 (2000).